

The Supernova — Supernova Remnant Connection

Dan Milisavljevic and Robert A. Fesen

Abstract Many aspects of the progenitor systems, environments, and explosion dynamics of the various subtypes of supernovae are difficult to investigate at extragalactic distances where they are observed as unresolved sources. Alternatively, young supernova remnants in our own galaxy and in the Large and Small Magellanic Clouds offer opportunities to resolve, measure, and track expanding stellar ejecta in fine detail, but the handful that are known exhibit widely different properties that reflect the diversity of their parent explosions and local circumstellar and interstellar environments. A way of complementing both supernova and supernova remnant research is to establish strong empirical links between the two separate stages of stellar explosions. Here we briefly review recent progress in the development of supernova—supernova remnant connections, paying special attention to connections made through the study of “middle-aged” ($\sim 10\text{--}100$ yr) supernovae and young (< 1000 yr) supernova remnants. We highlight how this approach can uniquely inform several key areas of supernova research, including the origins of explosive mixing, high-velocity jets, and the formation of dust in the ejecta.

1 Introduction

Distant extragalactic supernovae (SNe) appear as unresolved point sources. This inescapable fact severely restricts our ability to investigate SNe in fine

Dan Milisavljevic
Harvard-Smithsonian Center for Astrophysics, 60 Garden St., Cambridge, MA 02138,
e-mail: dmilisav@cfa.harvard.edu

Robert A. Fesen
Dartmouth College, 6127 Wilder Laboratory, Hanover, NH 03755, e-mail:
robert.fesen@dartmouth.edu

detail, and introduces a fundamental obstacle to obtaining three-dimensional kinematic and chemical data about the expanding ejecta that can be used to extract key properties of the progenitor star system and the explosion processes associated with the supernova.

One way around this problem is to examine young, nearby supernova remnants (SNRs) that encode valuable information in their expanding debris and evolution. Investigations of SNRs offer opportunities to resolve, measure, and track the expanding stellar ejecta, which in turn provides detailed information about the explosion dynamics, nucleosynthetic yields, and mixing of the progenitor star's chemically distinct layers. Additionally, the progenitor star system's evolutionary stages and mass-loss can be explored by studying the SN's interaction with its surrounding environment, and the fate of the SN's remnant core can be deduced through observations of central compact objects (CCOs).

However, SNR investigations come with their own set of limitations. With increasing age, interpretations of debris fields are complicated by the SN's increasing interaction with local environments. Observed asymmetry in SN morphology may be due to an inhomogeneous circumstellar and/or interstellar mediums (CSM/ISM), or non-spherical explosion. Consequently, the number of suitable objects of investigation where these types of effects are minimal is relatively small.

Establishing links between the variety of extragalactic SNe seen and the diverse collection of young, nearby and resolved SNRs is a way of complementing both areas of research. SN studies provide data on diversity and rates of SN types and subclasses as well as peak mean ejection velocities of chemically distinct layers, while SNRs provide detailed three dimensional kinematic and chemical information of the ejecta and progenitor star mass loss distribution. Here we give a brief overview of progress made at establishing connections between SNe and SNRs.

2 The Remnants of Historical Galactic Supernovae

Although there are about 300 SNRs identified in the Milky Way, less than a dozen are $\lesssim 1000$ years old (Green 2014). Young remnants are particularly useful for establishing SN-SNR connections because they have not been diluted by interaction with their local circumstellar and interstellar mediums (CSM/ISM) and exhibit properties still reflective of the type of SN from which they originated. Especially young Galactic remnants have the added advantage that many have been linked to historically witnessed celestial events (Clark & Stephenson 1977).

Modern classification of SNe follows a system based on the lack or presence of spectral lines seen at optical wavelengths around the time of explosion when the SN is most luminous. The primary division is made between Type I and

II events, first proposed by Minkowski (1941). Type I SNe lack conspicuous features associated with hydrogen and Type II SNe show clear hydrogen lines. Decades of SN discovery has uncovered a zoo of events of diverse spectral properties and luminosities (Filippenko 1997; Gal-Yam 2012). The two major divisions of SNe are now generally differentiated by the types of explosive progenitor stars: thermonuclear explosions of white dwarfs (Type Ia) and core collapses of massive ($> 8 M_{\odot}$) stars (Type II, II_n, II_b, Ib, and Ic).

The far broader range of observed properties in core-collapse SNe compared to SN Ia reflect both a wider range of progenitor masses and the loss of a hydrogen and/or helium rich envelope at the time of outburst (Filippenko 1997). This diversity of high mass progenitors and SN subtypes is in contrast to just three main types of young SNRs: O-rich remnants like Cassiopeia A (Cas A), pulsar dominated or so-called plerion remnants like the Crab Nebula, and collisionless shock dominated remnants like Tycho’s SNR.

Early attempts at relating SN types with SN remnants involved connecting SNRs with historical records of “guest stars” (Clark & Stephenson 1977). Because these ancient sightings provide no information about the spectroscopic properties of the events, and offer scant and sometimes questionable information about the SN’s peak brightness, color, and duration of visibility (Schaefer 1996; Fesen et al. 2012), they are limited in their ability to relate young Milky Way remnants to extragalactic SNe.

Most young galactic SNRs have strong individual characteristics that are not always shared by other young SNRs or easily connected to SN subclasses. Such differences largely arise from the role CSM can play in affecting a remnant’s properties and evolution. For example, the young galactic remnant Cas A shows optical properties unlike most of the other O-rich SNRs for which it is suppose to be the prototype. The galactic remnant W50/SS433 and the O-rich ejecta + 50 msec pulsar remnant 0540-69 in the LMC also defy the three simple cataloging classes.

However, recent studies at X-ray wavelengths have provided reasonably good methods for differentiating Type Ia remnants from remnants of core-collapse SNe. These methods of analyses include estimates of iron abundance (Reynolds et al. 2007), X-ray line morphologies (Lopez et al. 2009), and Fe-K line energy centroids (Patnaude et al. 2015). In some cases these analyses are able to provide SN subclassifications (Patnaude et al. 2012). Unfortunately, in most cases Galactic remnants are too old for such methods to provide this level of detail.

The famous Crab Nebula is an example of the difficulty of connecting a SNR with a particular type of extragalactic SN. Although from ancient records we know its precise age and peak visual brightness, the historic SN of 1054 AD left a remnant unlike any other in our galaxy. With an expansion velocity ($< 2000 \text{ km s}^{-1}$) far lower than commonly seen in SNe, an extremely luminous pulsar, and ejecta showing only helium enrichment – and even then only in a select band of filaments – debate continues as to which

SN subtype best matches its properties (Davidson & Fesen 1985; Smith 2013; Yang & Chevalier 2015).

Robust connections between various SN types and young SNRs have recently been achieved through the study of SN light echos. Light from the SN scattered by interstellar dust can be observed after a time delay resulting from a longer path length. Spectroscopy of these light echoes has led to robust SN associations between the young Milky Way and LMC/SMC remnants 0509-67.5 and Tycho with SN Ia events (Rest et al. 2008; Krause et al. 2008a). Similarly, Cas A has been associated with the Type IIb SN 1993J (Krause et al. 2008b; Rest et al. 2011), which is discussed in detail in Section 6.

3 The SN to SNR Transition

There is no generally accepted definition for the point when a SN becomes a SNR. A theoretical definition is that the remnant phase begins when a SN departs from free expansion and begins to strongly interact with its surrounding ISM. On the other hand, an operational definition might be when both UV/optical line and continuum emission from a SN's ejecta falls below that generated by interaction with either surrounding CSM/ISM material or via emission from a central compact stellar remnant (Fesen 2001). However, these definitions are not applicable for Type IIn SNe that exhibit strong SN-CSM interaction immediately after explosion and may represent $\sim 10\%$ of core-collapse explosions (Smith et al. 2011).

While monitoring the evolution of a SN from explosion into a young remnant over timescales of $10^2 - 10^3$ yr is not practical, timescales of decades are short enough to permit SN-SNR connections. This was first recognized in the late 1980s with the optical re-detections of SN 1980K (Fesen & Becker 1988) and SN 1957D (Long et al. 1989), and on-going studies of SN 1987A in the LMC have been helpful in allowing us to witness certain aspects of this identity change. However, the particular properties of any one intermediate- or "middle"-aged SN do not offer the desired broad insights about the formation and evolution of young remnants across the whole spectrum of SN subclasses. To accomplish this, examinations of a variety of well-evolved SNe is required.

Detections of SNe passing through the transitional state into remnants are relatively rare. This is chiefly a consequence of their fairly rapid decline in luminosity. Because the majority of SNe occur at distances > 10 Mpc and fade at least eight magnitudes below peak brightness in their first two years, observations have been largely limited to one year or so after maximum light when they are at apparent magnitudes < 20 .

Fortunately, favorable circumstances sometimes make it possible to monitor SNe many years or even decades post-outburst. In the special case of

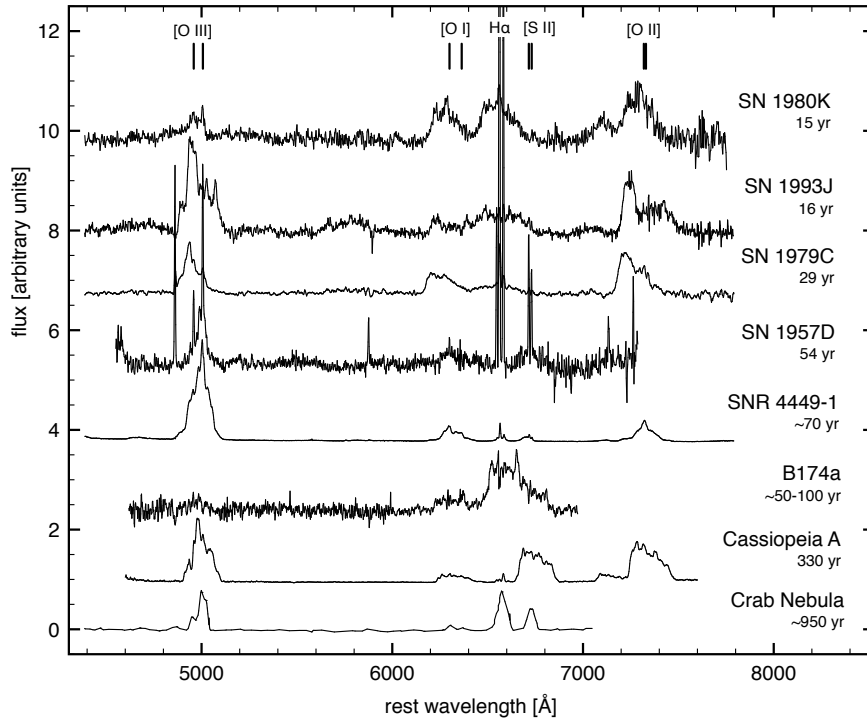


Fig. 1 Several well-observed middle-aged SNe and two spatially integrated spectra of young SNRs. Data have been originally published in the following papers: SN 1979C (Milisavljevic et al. 2009); SN 1957D (Long et al. 2012); B174a (Blair et al. 2015); SNR 4441-1 (Milisavljevic & Fesen 2008); Crab Nebula (Smith 2003); all others are from Milisavljevic et al. (2012).

SN 1987A, its close proximity in the LMC has enabled long-term monitoring. In the majority of other cases when late-time monitoring is possible, some long-lived energy source related to interaction between the SN and ISM/CSM or a CCO maintains optical luminosity at observable levels. Because young Type Ia remnants do not appear to undergo strong ISM or CSM interactions and do not contain CCOs, the majority of recent SN–SNR studies have concentrated on core-collapse SNRs. Accordingly, this chapter focuses on core-collapse events. Exceptional cases of middle-aged Type Ia observations do exist, however, such as G1.9 + 0.3 (Borkowski et al. 2014), and SN 1885, which we highlight in Section 9.

Figure 1 shows a sample of well-observed late-time emissions (i.e., “nebular spectra”) of core-collapse SNe. The figure has been modified from Milisavljevic et al. (2012) to include the recent discovery of a very young SNR by Blair et al. (2015) during a survey of M83, and a superior deep optical spectrum of SN 1957D by Long et al. (2012). Also shown in the figure

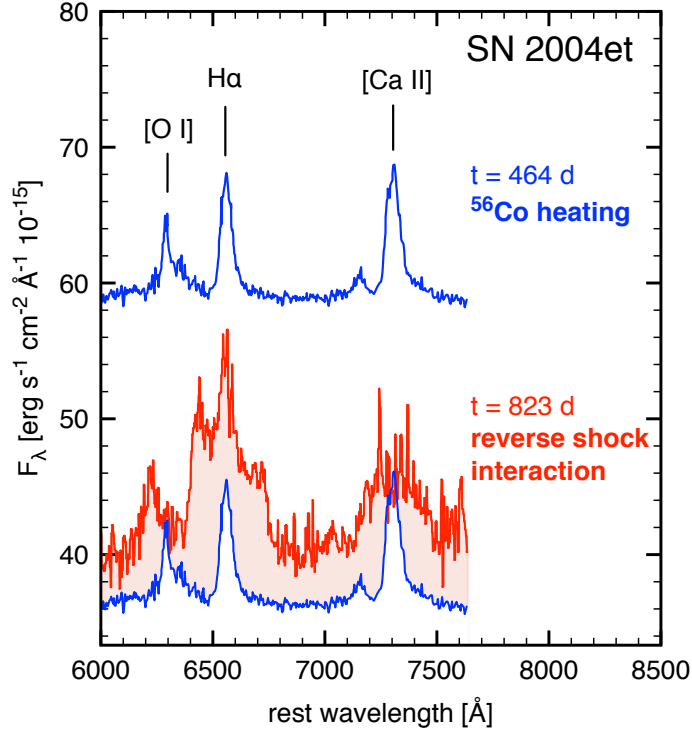


Fig. 2 Optical spectra of SN 2004et from Kotak et al. (2009). At $t = 464$ d, the emission from the [O I], H α and [Ca II] lines are powered by radioactive ^{56}Co , which was originally ^{56}Ni synthesized in the explosion and mixed from interior regions. At $t = 823$ d, the emission line profiles of these ions undergo a dramatic broadening, from $V \sim 3000$ km s $^{-1}$ to $V \sim 8500$ km s $^{-1}$, which is consistent with the reverse shock exciting outer, higher velocity ejecta. Emission around [Ca II] at $t = 823$ d may have a contribution from [O II].

are spatially integrated spectra of two young supernova remnants: Cas A (Milisavljevic et al. 2012) and the Crab Nebula (Smith 2003).

As shown in Figure 1, there is great variety in the late-time optical spectra of middle-aged core-collapse SNe, seen mostly in the relative line strengths and expansion velocities of [O I] $\lambda\lambda 6300, 6364$, [O II] $\lambda\lambda 7319, 7330$, [O III] $\lambda\lambda 4959, 5007$, [S II] $\lambda\lambda 6716, 6731$, and H α . Nonetheless, important trends that reflect fundamental properties of these systems do emerge upon close inspection. We discuss these trends in the next section.

4 Energy Sources of Late-time Emission

Of the various late-time mechanisms theorized to power SN emission at epochs > 2 yr, the most common process is the forward shock front and SN ejecta interaction with surrounding CSM shed from the progenitor star (see Chevalier & Fransson 2003 and references therein). These SN–CSM interactions lead to the formation of a reverse shock moving back into the expanding ejecta, which may subsequently ionize a broad inner ejecta region from which the optical lines are produced. Other proposed late-time mechanisms include pulsar/magnetar interaction with expanding SN gas (Chevalier & Fransson 1992; Woosley 2010) or accretion onto a black-hole remnant (Patnaude et al. 2011).

The point at which SN–CSM interaction leading to reverse shock-heating of inner ejecta dominates observed optical emission ranges widely. For most core-collapse SNe, the timescale is at least 1–2 yr. The timescale is dominated by the dynamics of the explosion and the local CSM/ISM environment it is running into. Prior to the initiation of SN–CSM interaction, emission is dominated by inner metal-rich ejecta that is excited from radioactive decay of $^{56}\text{Ni} \rightarrow ^{56}\text{Co} \rightarrow ^{56}\text{Fe}$.

The SN–SNR transition between radioactive ^{56}Co heating of O-rich ejecta from the interior (directed outward) to reverse shock excitation from the exterior (directed inward) is illustrated in Figure 2. Two epochs of late-time spectra of SN 2004et (originally presented in Kotak et al. 2009) show a substantial increase in the width of the emission line profiles of [O I], [Ca II], and $\text{H}\alpha$. This transformation is best understood as the consequence of the reverse shock beginning to strongly interact with metal-rich ejecta. Such an abrupt change in emission is rarely observed in SNe but is an important step in the transition from SN to SNR.

The various mechanisms of late-time emission can be distinguished via observed changes in velocity widths of emission line profiles (Chevalier & Fransson 1992, 1994). In circumstellar interaction scenarios where the reverse shock penetrates into deeper layers of ejecta, the velocity widths of emission lines are expected to narrow with time. Changes in relative line strengths are also anticipated as expansion drives down ejecta density. The flux ratio $[\text{O III}]/([\text{O I}]+[\text{O II}])$ increases with time and $\text{H}\alpha/([\text{O I}]+[\text{O II}])$ should decrease (Figure 3). Alternatively, in scenarios involving a pulsar wind nebula where emission is powered by photoionization, line widths are anticipated to broaden because of acceleration by the pulsar wind bubble.

The extragalactic SNe shown in Figure 1 all exhibit the anticipated changes in emission line strengths and widths attributable to SN–CSM interaction at optical wavelengths. However, some of these SNe show signs of hosting pulsar wind nebulae or black holes at X-ray wavelengths. For example, the X-ray flux density of SN 1970G recently increased by a factor of ~ 3 while its radio flux significantly lowered (Dittmann et al. 2014). This might be due to the turn-on of a pulsar wind nebula. Similarly, SN 1957D was recently

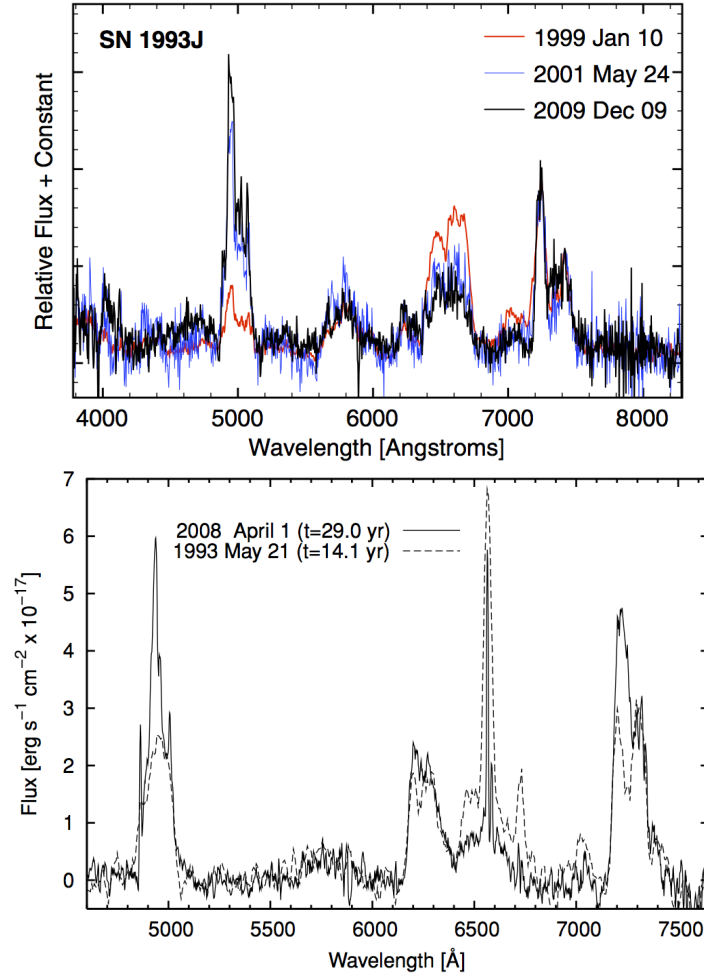


Fig. 3 Emission evolution in middle-aged SNe. Top: Three epochs of optical spectra of the Type IIb SN 1993J showing the evolution of relative line strengths (Milisavljevic et al. 2012). Bottom: Two epochs of optical spectra of the Type IIL SN 1979C (Milisavljevic et al. 2009). Declining $H\alpha$ emission with simultaneous increasing $[O III]$ emission is apparent, which is commonly observed in late-time emissions of SNe as ejecta continue to expand and cool and the reverse shock penetrates through the H-rich layers of the ejecta.

re-detected at X-ray wavelengths showing a hard and highly self-absorbed spectrum which suggests the presence of an energetic pulsar and its pulsar wind nebula (Long et al. 2012). Perhaps most remarkable is the constant X-ray luminosity of SN 1979C that possibly signals emission powered by either a stellar-mass ($5 - 10 M_{\odot}$) black hole accreting material or a central pulsar wind nebula (Patnaude et al. 2011).

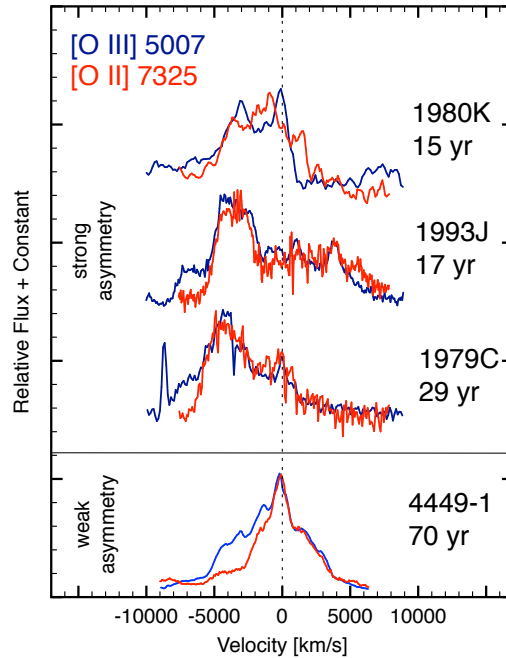


Fig. 4 Strong and weak emission line asymmetry in middle-aged SNe. Velocities of [O III] 4959, 5007 emission line profiles are with respect to 5007 Å. Velocities of [O II] 7319, 7330 emission line profiles are with respect to 7325 Å. Adapted from Milisavljevic et al. (2012).

5 Emission Asymmetry

Asymmetric emission line profiles are common in late-time core-collapse SN spectra. In Figure 4, we show three examples of emission asymmetry in the [O III] $\lambda\lambda 4959, 5007$ line profiles of SN 1980K, SN 1993J, and SN 1979C. The blue-red asymmetry (i.e., most emission is observed at blueshifted velocities) tends to be strongest in the forbidden oxygen lines, but can also be observed in $H\alpha$, [S II], and [Ar III] line profiles. Hubble Space Telescope (*HST*) observations of SN 1979C have shown that this asymmetry can be even stronger at UV wavelengths (Fesen et al. 1999). A small subset of SNe do not exhibit pronounced asymmetry in their emission line profiles, or exhibit a mixed combination of profiles that both do and do not show asymmetry. For example, the ultraluminous oxygen-rich SNR 4449-1 shows mild asymmetry in its oxygen emission, but strong blue asymmetry in its [S II] $\lambda\lambda 6716, 6731$ and [Ar III] $\lambda 7136$ emission profiles with blueshifted velocity distributions spanning $-2500 < V_{\text{exp}} < 500 \text{ km s}^{-1}$ (Milisavljevic & Fesen 2008; Bietenholz et al. 2010).

These asymmetric oxygen emission line profiles indicate that internal absorption is obscuring emission from the SN’s receding rear hemisphere. Dust formation in the metal-rich ejecta is a principal cause of this type of absorption at late epochs. Alternatively, absorption by dust may take place in the cool dense shell (CDS) in the shock region (Deneault et al. 2003). This is a likely place for dust formation because of its high density and low temperature (Chevalier & Fransson 1994). These emission line asymmetries can be modeled to estimate dust composition and mass. For example, Bevan & Barlow (2016) modeled the late-time H α and [O I] line emission profiles of SN 1987A. Their results confirmed a steady increase in the dust mass in SN 1987A’s ejecta, from $< 3 \times 10^{-3} M_{\odot}$ on day 714 to $> 0.1 M_{\odot}$ by day 3604 (but see also Dwek & Arendt 2015). This time-dependent dust mass growth is relevant to understanding the extent to which core-collapse SNe contribute to the high quantities of dust observed in some high redshift galaxies (Watson et al. 2015).

In addition to the blue-red emission asymmetry, oxygen line profiles of extragalactic SNe also show conspicuous emission line substructure. This substructure, which comprises minor emission peaks that can last many years (> 10), is typically interpreted as “blobs” or “clumps” of material. Their presence and longevity suggests that they are associated with regions of emitting material that represent a large fraction of the entire optically-emitting SN.

Large clumps are consistent with aspheric SN explosions with turbulent mixing. Theory and observation strongly favor the notion that asymmetric explosions drive core-collapse SNe. However, where and how this asymmetry is introduced is uncertain. Some explosion asymmetries are potentially introduced by dynamical instabilities and the influences of rotation and magnetic fields (Akiyama et al. 2003; Janka 2012; Burrows 2013), while others may be introduced by a perturbed progenitor star structure (Arnett & Meakin 2011; Couch & Ott 2013; Wongwathanarat et al. 2015). In the next section we explore how the robust SN–SNR connection between SN 1993J and Cas A has provided powerful insight into the physical origins of emission line asymmetry and substructure.

6 The Cassiopeia A—SN 1993J Connection

Cas A is considered the prototype for the class of young, oxygen-rich SNRs and provides a clear look at the explosion dynamics of a core-collapse SN. Cas A’s distance of 3.4 kpc (Reed et al. 1995) has permitted detailed study of its composition and distribution of SN ejecta on fine scales, and its estimated current age of ≈ 340 yr (Thorstensen et al. 2001; Fesen et al. 2006) places it at a stage of evolution not that different from middle-aged SNe (Fig. 1).

Cas A probably originated from a red supergiant progenitor with mass $10 - 30 M_{\odot}$ that may have lost much of its hydrogen envelope to a binary

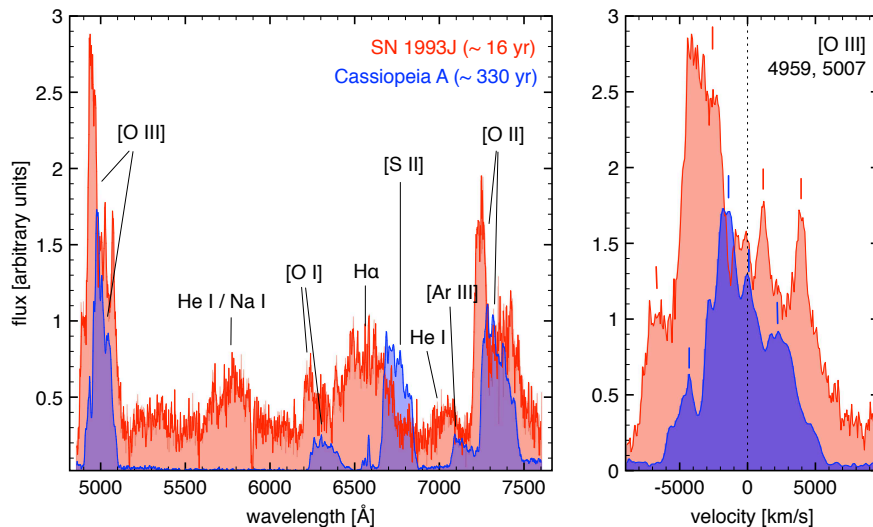


Fig. 5 Spatially integrated optical spectrum of Cas A compared to that of SN1993J (modified from Milisavljevic et al. 2012). The left panel shows the entire spectrum with dominant emission features identified. The right panel shows an enlargement around the [O III] emission line profile. Solid lines highlight long-lasting emission line substructure.

interaction (Chevalier & Oishi 2003; Young et al. 2006). Spectroscopy of optical echoes of the SN outburst indicate that the original SN of Cas A was of Type IIb (Krause et al. 2008b) and showed strong evidence for asymmetry in the explosion (Rest et al. 2011). The integrated spectrum of the Cas A SNR is similar to many of the middle-aged CCSNe exhibiting strong [O III] emission. Particularly well-matched with Cas A are SN 1979C, SNR 4449-1, SN 1980K, and SN 1993J.

In Figure 5, the optical spectra of Cas A and SN 1993J are compared directly. Also shown in Figure 5 are the [O III] emission line profiles enlarged. Conspicuous minor emission peak substructure common to the two spectra is highlighted. The differences and similarities between the two are of especial interest given that Cas A’s Type IIb classification was made by comparing its light echo spectra to that of SN 1993J near maximum light (Krause et al. 2008b; Rest et al. 2011). Together, the two spectra illustrate the evolution of a Type IIb explosion from decades to centuries after explosion. Three key properties of the evolution reflect the reverse shock’s progression toward the inner layers of the ejecta: 1) The strength of $H\alpha$ emission decreases as the H-rich outer layers of the ejecta are overtaken. 2) The velocity of the emission line profile decreases. 3) Sulfur emission is visible only after the reverse shock has penetrated into the inner S-rich layers of the debris.

Both Cas A and SN 1993J show excess emission at blueshifted velocities. Resolved multi-wavelength observations of Cas A suggest that this emission

asymmetry is the result of absorption due to dust in the ejecta. In particular, infrared studies of Cas A have estimated that upwards of $0.05 M_{\odot}$ of dust reside in its shocked ejecta (Rho et al. 2008). Thus, the same mechanism likely also applies for SN 1993J. This SN–SNR connection is consistent with notion that that dust formation processes are significant when the reverse shock starts to excite ejecta in the first few years post-explosion, and last for centuries later.

The young age of Cas A and minimal influence of SN–CSM interaction has kept its ejecta in ballistic trajectories from a well established center of expansion (Thorstensen et al. 2001). This unique property has enabled three dimensional reconstructions of the remnant at optical (Reed et al. 1995; Milisavljevic & Fesen 2013), and infrared and X-ray wavelengths (DeLaney et al. 2010). Milisavljevic & Fesen (2013) conducted a high-resolution optical survey of Cas A that included its highest velocity ejecta in the NE and SW outflows sometimes called “jets” (see Section 8). They found that the majority of the optical ejecta are arranged in several well-defined and nearly circular ring-like structures with diameters between approximately $30''$ (0.5 pc) and $2'$ (2 pc) (see Figure 6).

In light of the many connections between Cas A and SN 1993J, the emission line substructure shared between them likely results from a common origin. If so, then the “clumps” of material often observed in late-time spectra of core-collapse SNe are not random, but instead associated with multi-ringed distributions of ejecta like that seen and resolved in Cas A. Strong evidence in support of this shared morphology comes from kinematic reconstructions of other young SNRs such as 1E 0102.2-7219 (Eriksen et al. 2001) and N132D (Vogt & Dopita 2011), which also exhibit ejecta arranged in ring-like geometries.

7 Ejecta Bubbles and Large-Scale Mixing

A near-infrared spectroscopic survey of Cassiopeia A’s interior unshocked S-rich material recently uncovered a bubble-like morphology that smoothly connects with the multi-ringed structures seen in the bright reverse shocked main shell of expanding debris (Figure 7; Milisavljevic & Fesen 2015). These bubbles were most likely created early in the explosion from plumes of radioactive ^{56}Ni -rich ejecta that decayed into cobalt and iron, releasing energy that would cause the gas to expand and compress nearby non-radioactive material such as oxygen, sulfur, and argon into cavity walls. Doppler mapping of the X-ray bright Fe-K emission in Cas A has shown that three regions of Fe-rich material sits within three of these rings (DeLaney et al. 2010; Milisavljevic & Fesen 2013), which is consistent with this proposed origin of the bubbles.

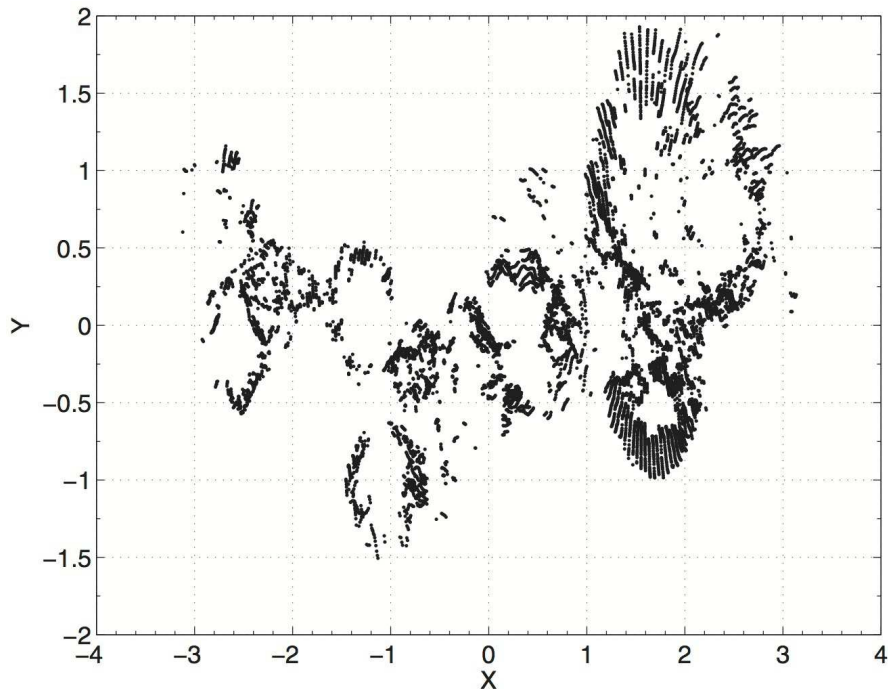


Fig. 6 The main shell of Cas A’s reverse-shocked optically emitting ejecta as represented in a Mercator projection. At least six rings are observed. The largest ring located in the northwest is approximately twice the size of the other rings. The cylindrical map projection distorts the size and shape of large objects, especially toward the poles. Adapted from Milisavljevic & Fesen (2013).

Compelling evidence for large-scale mixing involving considerable non-radial flow and the development of “Ni-bubbles” was first observed in SN 1987A. In that case, high energy gamma-rays and X-rays with broad emission line widths from the decay of ^{56}Ni were detected only months after the explosion, implying that Ni-rich material was near the star’s surface well before 1D progenitor models had predicted assuming spherical symmetry (Pinto & Woosley 1988; Li et al. 1993).

Since SN 1987A, state-of-the-art 3D computer simulations of core-collapse explosions have confirmed that large-scale mixing originating from uneven neutrino heating can lead to Ni-dominated plumes overtaking the star’s outer oxygen- and carbon-rich layers with velocities up to 4000 km s^{-1} (Hammer et al. 2010). However, the majority of these simulations show that the mass density should essentially be unaffected. Though mixing affects the species distribution, the bulk of the Ni mass should remain inside the remnant with velocities below 2000 km s^{-1} . This is, in fact, opposite to what is seen in Cas A, where the X-ray bright Fe has velocities around and above the 4000

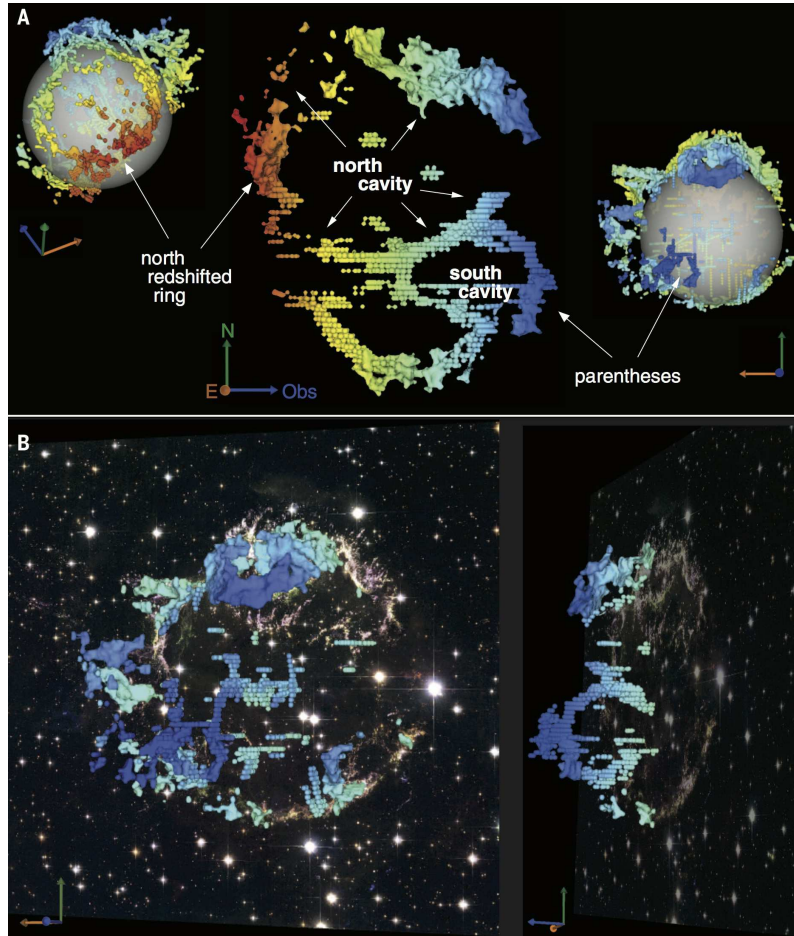


Fig. 7 Doppler reconstruction of Cas A. The blue-to-red color gradient corresponds to Doppler velocities that range from -4000 to $+6000$ km s^{-1} . (A) A side perspective of a sliced portion of the remnant chosen to emphasize two conspicuous interior cavities and their connections to main-shell ejecta. The translucent sphere centered on the origin of expansion is a visual aid to differentiate between front and back material. (B) Two angled perspectives highlighting the south cavity. Adapted from Milisavljevic & Fesen (2015).

km s^{-1} limit. Thus, either the simulations are not adequately following the dynamics of mixing, or more Fe remains to be detected in Cas A's interior. This latter scenario is somewhat problematic. Approximately $0.1 M_{\odot}$ of Fe (the decay product of Ni) is presently observed in Cas A (Hwang & Laming 2012), and yet the total amount produced in the original SN is believed to have been less than this (Eriksen et al. 2009).

An additional consideration in interpreting a SN debris field is the chemical make-up of the star at the time of outburst. The evolution of massive

stars toward the ends of their life cycles is likely to be non-spherical and may have extensive inter-shell mixing. If strong enough, these dynamical interactions lead to Rayleigh-Taylor instabilities in the progenitor structure that can influence the overall progression of the explosion and contribute to the formation of Ni-rich bubbles (Arnett & Meakin 2011). Thus, asymmetries introduced by a turbulent progenitor star interior in addition to those initiated by the explosion mechanism may contribute to bubble-like morphologies.

8 Jet Activity in Core-collapse Supernovae

Interestingly, a continuum of explosion energies extending from broad-lined Type Ic SNe associated with gamma-ray bursts, to more ordinary Type Ib/c SNe appears to exist (Soderberg et al. 2010). Such events suggest that a wide variety of jet activity may potentially be occurring at energies that are hidden observationally (Margutti et al. 2014; Milisavljevic et al. 2015). In these cases, the central engine activity stops and becomes “choked” before the jet is able to pierce through the stellar envelope. SNe associated with choked jets lack sizable amounts of relativistic ejecta and thus can be dynamically indistinguishable from ordinary core-collapse SNe (Lazzati et al. 2012).

Whether or not an internal jet successfully emerges from a star experiencing a SN explosion is dependent on many factors. Perhaps the most important factor is core rotation at the time of core collapse. For the majority of SNe, rotation effects are anticipated to be small and the explosion neutrino-driven. However, in a small subset of cases where core rotation of the pre-SN star is rapid, magnetic fields will be amplified and make magnetohydrodynamic (MHD) power influential (Akiyama et al. 2003). In these extreme cases where the rotation rate is very fast, MHD processes may dominate and a hypernova and/or a GRB could result (Burrows et al. 2007). Another factor is the progenitor star size and composition. Large stellar envelopes and/or He layers may inhibit central jets from completely piercing the surface of the star (see, e.g., Mazzali et al. 2008).

Searches for vestiges of prior SN jet activity in SNRs have had largely inconclusive and/or debated conclusions. For example, the Crab has a curious filamentary feature that is $45''$ wide and extends approximately $100''$ off the nebula’s northern limb. Whether this “jet” was strongly sculpted by the surrounding ISM or more directly influenced by the central pulsar has not been resolved. Most recently, Black & Fesen (2015) examined the Crab’s 3D filamentary structure along the jet’s base and found a large and nearly emission-free opening in the remnant’s thick outer ejecta shell. The jet’s blueshifted and redshifted sides are surprisingly well defined and, like the jet’s sharp western limb, appear radially aligned with the remnant’s center of expansion.

Another example is the SNR W49B. Lopez et al. (2013) conclude that the morphological, spectral, and environmental characteristics of W49B are indicative of a bipolar Type Ib/Ic SN explosion. However, the arguments in favor of a jet-induced explosion for this fairly evolved remnant that is known to be interacting with a nearby molecular cloud are largely circumstantial. Optical and near-infrared spectroscopy has been unable to detect any emission attributable to high velocity metal-rich ejecta that could provide direct confirmation of a jet-driven explosion.

On the other hand, Cas A exhibits exceptionally high velocity Si- and S-rich material in a jet/counter-jet arrangement (Fesen 2001; Hwang et al. 2004). The known extent of this jet region contains fragmented knots of debris traveling $\sim 15,000 \text{ km s}^{-1}$, which is three times the velocity of the bulk of the O- and S-rich main shell. Although the large opening half-angle of this high-velocity ejecta is inconsistent with a highly collimated flow (Fesen 2001; Milisavljevic & Fesen 2013), and spatial mapping of radioactive ^{44}Ti emission appears to rule out a jet-induced bipolar explosion (Grefenstette et al. 2014), some jet-like mechanism carved a path allowing interior material from the Si-S-Ar-Ca region near the core out past the mantle and H- and He-rich photosphere (Fesen & Milisavljevic 2016).

Given that the energy associated with the NE/SW jets of Cas A is below the energy anticipated to be associated with the original SN explosion, an observational signature of their presence would be hidden at extragalactic distances. The same is true for the Crab Nebula. Only through nearby, resolved inspection is the existence of these structures recognizable.

9 The SN 1885—SN Ia Connection

In contrast with core-collapse SNe that produce CCOs and undergo strong ISM/CSM interactions that can energize observable levels of late-time emissions, normal Type Ia SNe completely disrupt their progenitor white dwarf stars and explode in relatively “clean” environments. Thus, after only a few years of free expansion, the ejecta cool adiabatically and become effectively invisible via line emission at extragalactic distances. This largely explains why late-time optical detections of Type Ia SNe are rare.

However, in exceptional circumstances, it has been possible to observe late-time *absorptions* from middle-aged extragalactic Type Ia SNe. This possibility was first realized with the re-detection of SN 1885 by Fesen et al. (1989). SN 1885 was a bright historical nova (also known as S And) discovered in late August of 1885 and located at a projected distance of $16''$ away from the nucleus of M31. The optical spectrum, colors, and light curve evolution have suggested SN 1885 to be a subluminous Type Ia SN (de Vaucouleurs & Corwin 1985), although this classification is uncertain (Perets et al. 2011). SN 1885’s

advantageous close proximity to Andromeda’s central bulge stars made it possible to observe the remnant’s ejecta via resonance line absorption.

High resolution observations of SN 1885 obtained with *HST* have been used to map the distribution of ejecta that are contained within a $\approx 0.75''$ diameter (Figure 8). Because the debris are still in near-free expansion after 130 yr, they retain the density distribution established shortly after the explosion and can provide valuable kinematic information about the general properties and character of a Type Ia explosion.

HST Fe II images of SN 1885 uncovered four plumes of Fe-rich material that extend from the remnant’s center out to $\approx 10^4$ km s $^{-1}$. This distribution stands in strong contrast with the distribution of Ca-rich material that is concentrated in a clumpy, broken shell spanning velocities of 1000 – 5000 km s $^{-1}$ but extends out to 12,500 km s $^{-1}$. Fesen et al. (2015) find that the observed distributions of ejecta are consistent with delayed detonation white dwarf models, and inconsistent with a highly anisotropic explosion that could result from a violent merger of two white dwarfs.

10 Conclusions

In this chapter, we have reviewed how several important properties of SN progenitor systems and explosion dynamics can be investigated through connections between the many unresolved extragalactic SNe and the few, resolved young SNRs seen in our galaxy, the Large and Small Magellanic Clouds, and Andromeda.

Although observations of late-time optical emissions from Type Ia SNe during the transitional middle-aged phase have not been possible, the unique case of SN 1885 has shown that the 2D arrangement of unshocked Fe-rich and Ca-rich debris is most consistent with delayed detonation white dwarf models. The plumes of Fe-rich material in this remnant may explain the Fe II emission line asymmetries commonly seen in late-time emission spectra of Type Ia SNe.

Middle-aged, core-collapse SNe powered by strong CSM interaction leading to reverse shock-heating of ejecta are especially helpful in making connections between SNe and SNRs. A particularly important SN–SNR connection is the Type IIb SN 1993J in M81 and the 340 year old O-rich galactic SNR Cassiopeia A.

Complex emission line substructures seen in SN 1993J and other core-collapse SNe typically interpreted as random “clumps” of material may, in fact, be more easily understood as large-scale rings of debris excited by a reverse shock like those seen in Cas A. These rings appear to be associated with a bubble-like interior originally caused by outwardly expanding plumes of radioactive ^{56}Ni -rich ejecta. Cas A’s bipolar jet-like features is consistent with the notion that a wide variety of jet activity may be occurring in core-

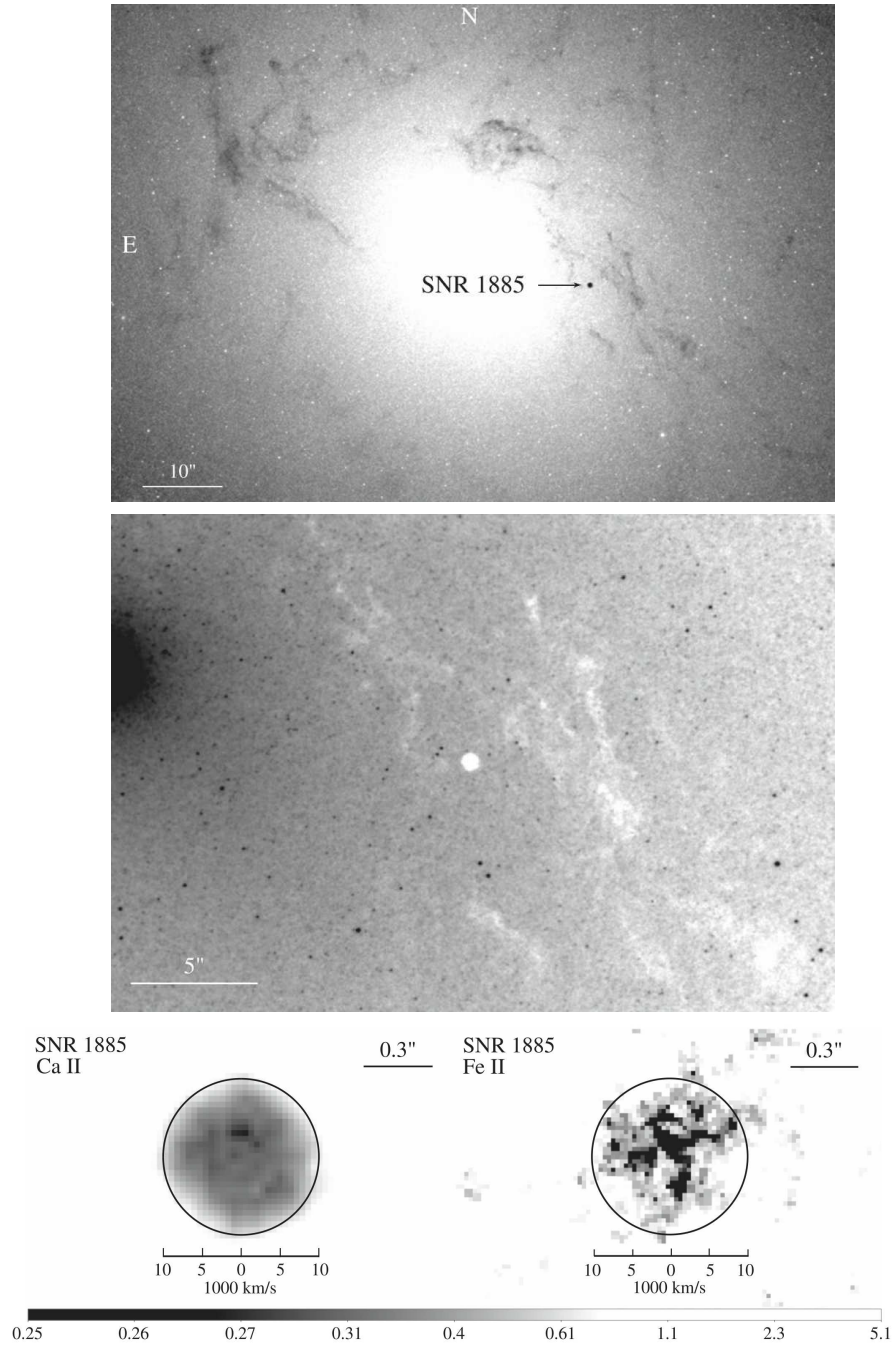


Fig. 8 *HST* observations of SN 1885. The top panel shows an WFC3 image of M31 taken with the F390M filter and displayed using a positive linear stretch. The location of SN 1885, which appears as round dark spot of Ca II H and K absorption, is marked. The middle panel shows an enlarged section of the same image centered on the SN and displayed using a negative log stretch. The bottom panels (left and right) show log intensity-stretched views of SN 1885 as seen in Ca II and Fe II images. Adapted from Fesen et al. (2015).

collapse SNe at energy scales that are observationally hidden at extragalactic distances.

The SN–SNR connections made through decades-long monitoring of recent SNe serve to emphasize the value of such observations. While high-quality late-time spectra are rare (less than 20 objects total), analysis of these data can reveal important and sometimes unexpected information. Furthermore, such SN–SNR connections can be used to uniquely test our theoretical understandings of SNe. Only through resolved inspections of SNRs can models of SNe be confronted with empirical facts and gain insight into crucial processes that may be lost in data obtained from unresolved extragalactic examples.

Finally, light echo spectroscopy has introduced a new and powerful tool for developing robust SN–SNR connections. It is anticipated that increasing success obtaining optical spectra of light echoes associated with historical Galactic SNe will continue to shed light on remnants that don't quite fit our current SN classifications, such as the Crab Nebula and Kepler. Moreover, the growing awareness that asymmetry plays a significant role in SN explosions provides strong motivation for 3D light echo spectroscopy, which has the unique capacity to yield information from multiple lines of sight.

Acknowledgments

We thank B. Blair, K. Long, and F. Winkler for providing data of B174a and SN1957D. A portion of this work was supported by NASA through grants GO-12300 and GO-12674 from the Space Telescope Science Institute (STScI), which is operated by the Association of Universities for Research in Astronomy.

Cross-References

- Historical records of supernovae
- Supernova of 1054 and its remnant, the Crab Nebula
- Supernova Remnant Cassiopeia A
- Observational Classification of Supernovae
- Hydrogen-Poor Core-Collapse Supernovae
- Nebular spectra of supernovae
- Explosion Physics of Core-Collapse Supernovae
- Neutrino Driven Explosions
- Non-spherical initial stellar structure and core collapse
- Dynamical Evolution and Radiative Processes of Supernova Remnants
- Galactic and Extragalactic Samples of Supernova Remnants: How They Are Identified and What They Tell Us

- Supernova remnant from SN1987A

References

- Akiyama, S., Wheeler, J. C., Meier, D. L., & Lichtenstadt, I. 2003, “The Magnetorotational Instability in Core-Collapse Supernova Explosions,” *ApJ*, 584, 954
- Arnett, W. D., & Meakin, C. 2011, “Toward Realistic Progenitors of Core-collapse Supernovae,” *ApJ*, 733, 78
- Bevan, A., & Barlow, M. J. 2016, “Modelling supernova line profile asymmetries to determine ejecta dust masses: SN 1987A from days 714 to 3604,” *MNRAS*, 456, 1269
- Bietenholz, M. F., Bartel, N., Milisavljevic, D., et al. 2010, “The first VLBI image of the young, oxygen-rich supernova remnant in NGC 4449,” *MNRAS*, 409, 1594
- Black, C. S., & Fesen, R. A. 2015, “A 3D kinematic study of the northern ejecta ‘jet’ of the Crab nebula,” *MNRAS*, 447, 2540
- Blair, W. P., Winkler, P. F., Long, K. S., et al. 2015, “A Newly Recognized Very Young Supernova Remnant in M83,” *ApJ*, 800, 118
- Borkowski, K. J., Reynolds, S. P., Green, D. A., et al. 2014, “Nonuniform Expansion of the Youngest Galactic Supernova Remnant G1.9+0.3,” *ApJL*, 790, L18
- Burrows, A. 2013, “Perspectives on core-collapse supernova theory,” *Reviews of Modern Physics*, 85, 245
- Burrows, A., Dessart, L., Livne, E., Ott, C. D., & Murphy, J. 2007, “Simulations of Magnetically Driven Supernova and Hypernova Explosions in the Context of Rapid Rotation,” *ApJ*, 664, 416
- Chevalier, R. A., & Fransson, C. 1992, “Pulsar nebulae in supernovae,” *ApJ*, 395, 540
- Chevalier, R. A., & Fransson, C. 1994, “Emission from circumstellar interaction in normal Type II supernovae,” *ApJ*, 420, 268
- Chevalier, R. A., & Fransson, C. 2003, “Supernova Interaction with a Circumstellar Medium,” *Supernovae and Gamma-Ray Bursters*, 598, 171
- Chevalier, R. A., & Oishi, J. 2003, “Cassiopeia A and Its Clumpy Presupernova Wind,” *ApJL*, 593, L23
- Clark, D. H., & Stephenson, F. R. 1977, “The historical supernovae,” Oxford [Eng.] ; New York : Pergamon Press, 1977. 1st ed.
- Couch, S. M., & Ott, C. D. 2013, “Revival of the Stalled Core-collapse Supernova Shock Triggered by Precollapse Asphericity in the Progenitor Star,” *ApJL*, 778, L7
- Davidson, K., & Fesen, R. A. 1985, “Recent developments concerning the Crab Nebula,” *Ann. Rev. Astr. Astrophys.*, 23, 119

- de Vaucouleurs, G., & Corwin, H. G., Jr. 1985, “S Andromedae 1885 - A centennial review,” *ApJ*, 295, 287
- DeLaney, T., Rudnick, L., Stage, M. D., et al. 2010, “The Three-dimensional Structure of Cassiopeia A,” *ApJ*, 725, 2038
- Deneault, E. A.-N., Clayton, D. D., & Heger, A. 2003, “Supernova Reverse Shocks: SiC Growth and Isotopic Composition,” *ApJ*, 594, 312
- Dittmann, J. A., Soderberg, A. M., Chomiuk, L., et al. 2014, “A Mid-life Crisis? Sudden Changes in Radio and X-Ray Emission from Supernova 1970G,” *ApJ*, 788, 38
- Dwek, E., & Arendt, R. G. 2015, “The Evolution of Dust Mass in the Ejecta of SN1987A,” *ApJ*, 810, 75
- Eriksen, K. A., Morse, J. A., Kirshner, R. P., & Winkler, P. F. 2001, “Fabry-Perot [O III] λ 5007 observations of the SMC oxygen-rich SNR 1E 0102-72.9,” *Young Supernova Remnants*, 565, 193
- Eriksen, K. A., Arnett, D., McCarthy, D. W., & Young, P. 2009, “The Reddening Toward Cassiopeia A’s Supernova: Constraining the ^{56}Ni Yield,” *ApJ*, 697, 29
- Fesen, R. A., & Becker, R. H. 1988, “Optical Detection of the Remnant of SN 1980K in NGC 6946,” *Bulletin of the American Astronomical Society*, 20, 962
- Fesen, R. A., Saken, J. M., & Hamilton, A. J. S. 1989, “Discovery of the remnant of S Andromedae (SN 1885) in M31,” *ApJL*, 341, L55
- Fesen, R. A., Gerardy, C. L., Filippenko, A. V., et al. 1999, “Late-Time Optical and Ultraviolet Spectra of SN 1979C and SN 1980K,” *AJ*, 117, 725
- Fesen, R. A. 2001, “An Optical Survey of Outlying Ejecta in Cassiopeia A: Evidence for a Turbulent, Asymmetric Explosion,” *ApJS*, 133, 161
- Fesen, R. A. 2001, “The SN-SNR connection,” *Young Supernova Remnants*, 565, 119
- Fesen, R. A., Hammell, M. C., Morse, J., et al. 2006, “The Expansion Asymmetry and Age of the Cassiopeia A Supernova Remnant,” *ApJ*, 645, 283
- Fesen, R. A., & Milisavljevic, D. 2016, “An HST Survey of the Highest-velocity Ejecta in Cassiopeia A,” *ApJ*, 818, 17
- Fesen, R. A., Höflich, P. A., & Hamilton, A. J. S. 2015, “The 2D Distribution of Iron-rich Ejecta in the Remnant of SN 1885 in M31,” *ApJ*, 804, 140
- Fesen, R. A., Kremer, R., Patnaude, D., & Milisavljevic, D. 2012, “The SN 393-SNR RX J1713.7-3946 (G347.3-0.5) Connection,” *AJ*, 143, 27
- Filippenko, A. V. 1997, “Optical Spectra of Supernovae,” *ARA&A*, 35, 309
- Gal-Yam, A. 2012, “Luminous Supernovae,” *Science*, 337, 927
- Green, D. A. 2014, “A catalogue of 294 Galactic supernova remnants,” *Bulletin of the Astronomical Society of India*, 42, 47
- Grefenstette, B. W., Harrison, F. A., Boggs, S. E., et al. 2014, “Asymmetries in core-collapse supernovae from maps of radioactive ^{44}Ti in Cassiopeia A,” *Nature*, 506, 339

- Hammer, N. J., Janka, H.-T., Müller, E. 2010, “Three-dimensional Simulations of Mixing Instabilities in Supernova Explosions,” *ApJ*, 714, 1371
- Hwang, U., Laming, J. M., Badenes, C., et al. 2004, “A Million Second Chandra View of Cassiopeia A,” *ApJL*, 615, L117
- Hwang, U., & Laming, J. M. 2012, “A Chandra X-Ray Survey of Ejecta in the Cassiopeia A Supernova Remnant,” *ApJ*, 746, 130
- Janka, H.-T. 2012, “Explosion Mechanisms of Core-Collapse Supernovae,” *Annual Review of Nuclear and Particle Science*, 62, 407
- Kotak, R., Meikle, W. P. S., Farrah, D., et al. 2009, “Dust and The Type II-Plateau Supernova 2004et,” *ApJ*, 704, 306
- Krause, O., Tanaka, M., Usuda, T., et al. 2008, “Tycho Brahe’s 1572 supernova as a standard type Ia as revealed by its light-echo spectrum,” *Nature*, 456, 617
- Krause, O., Birkmann, S. M., Usuda, T., et al. 2008, “The Cassiopeia A Supernova Was of Type IIb,” *Science*, 320, 1195
- Lazzati, D., Morsony, B. J., Blackwell, C. H., & Begelman, M. C. 2012, “Unifying the Zoo of Jet-driven Stellar Explosions,” *ApJ*, 750, 68
- Li, H., McCray, R., & Sunyaev, R. A. 1993, *ApJ*, 419, 824
- Long, K. S., Blair, W. P., & Krzeminski, W. 1989, “Discovery of optical emission from the remnant of SN 1957D in M83,” *ApJL*, 340, L25
- Long, K. S., Blair, W. P., Godfrey, L. E. H., et al. 2012, “Recovery of the Historical SN1957D in X-Rays with Chandra,” *ApJ*, 756, 18
- Lopez, L. A., Ramirez-Ruiz, E., Castro, D., & Pearson, S. 2013, “The Galactic Supernova Remnant W49B Likely Originates from a Jet-driven, Core-collapse Explosion,” *ApJ*, 764, 50
- Lopez, L. A., Ramirez-Ruiz, E., Badenes, C., et al. 2009, “Typing Supernova Remnants Using X-Ray Line Emission Morphologies,” *ApJ*, 706, L106
- Margutti, R., Milisavljevic, D., Soderberg, A. M., et al. 2014, “Relativistic Supernovae have Shorter-lived Central Engines or More Extended Progenitors: The Case of SN 2012ap,” *ApJ*, 797, 107
- Mazzali, P. A., Valenti, S., Della Valle, M., et al. 2008, “The Metamorphosis of Supernova SN 2008D/XRF 080109: A Link Between Supernovae and GRBs/Hypernovae,” *Science*, 321, 1185
- Milisavljevic, D., & Fesen, R. A. 2008, “The Nature of the Ultraluminous Oxygen-Rich Supernova Remnant in NGC 4449,” *ApJ*, 677, 306
- Milisavljevic, D., Fesen, R. A., Kirshner, R. P., & Challis, P. 2009, “The Evolution of Late-Time Optical Emission from SN 1979C,” *ApJ*, 692, 839
- Milisavljevic, D., Fesen, R. A., Chevalier, R. A., et al. 2012, “Late-time Optical Emission from Core-collapse Supernovae,” *ApJ*, 751, 25
- Milisavljevic, D., & Fesen, R. A. 2013, “A Detailed Kinematic Map of Cassiopeia A’s Optical Main Shell and Outer High-velocity Ejecta,” *ApJ*, 772, 134
- Milisavljevic, D., & Fesen, R. A. 2015, “The bubble-like interior of the core-collapse supernova remnant Cassiopeia A,” *Science*, 347, 526

- Milisavljevic, D., Margutti, R., Parrent, J. T., et al. 2015, “The Broad-lined Type Ic SN 2012ap and the Nature of Relativistic Supernovae Lacking a Gamma-Ray Burst Detection,” *ApJ*, 799, 51
- Minkowski, R. 1941, “Spectra of Supernovae,” *PASP*, 53, 224
- Patnaude, D. J., Loeb, A., & Jones, C. 2011, “Evidence for a possible black hole remnant in the Type IIL Supernova 1979C,” *New Astronomy*, 16, 187
- Patnaude, D. J., Badenes, C., Park, S., & Laming, J. M. 2012, “The Origin of Kepler’s Supernova Remnant,” *ApJ*, 756, 6
- Patnaude, D. J., Lee, S.-H., Slane, P. O., et al. 2015, “Are Models for Core-collapse Supernova Progenitors Consistent with the Properties of Supernova Remnants?,” *ApJ*, 803, 101
- Perets, H. B., Badenes, C., Arcavi, I., Simon, J. D., & Gal-yam, A. 2011, “An Emerging Class of Bright, Fast-evolving Supernovae with Low-mass Ejecta,” *ApJ*, 730, 89
- Pinto, P. A., & Woosley, S. E. 1988, “The theory of gamma-ray emergence in supernova 1987A,” *Nature*, 333, 534
- Reed, J. E., Hester, J. J., Fabian, A. C., & Winkler, P. F. 1995, “The Three-dimensional Structure of the Cassiopeia A Supernova Remnant. I. The Spherical Shell,” *ApJ*, 440, 706
- Rest, A., Matheson, T., Blondin, S., et al. 2008, “Spectral Identification of an Ancient Supernova Using Light Echoes in the Large Magellanic Cloud,” *ApJ*, 680, 1137
- Rest, A., Foley, R. J., Sinnott, B., et al. 2011, “Direct Confirmation of the Asymmetry of the Cas A Supernova with Light Echoes,” *ApJ*, 732, 3
- Reynolds, S. P., Borkowski, K. J., Hwang, U., et al. 2007, “A Deep Chandra Observation of Kepler’s Supernova Remnant: A Type Ia Event with Circumstellar Interaction,” *ApJL*, 668, L135
- Rho, J., Kozasa, T., Reach, W. T., et al. 2008, “Freshly Formed Dust in the Cassiopeia A Supernova Remnant as Revealed by the Spitzer Space Telescope,” *ApJ*, 673, 271
- Schaefer, B. E. 1996, “Peak Brightnesses of Historical Supernovae and the Hubble Constant,” *ApJ*, 459, 438
- Smith, N. 2003, “The integrated optical spectrum of the Crab nebula and evidence for its fading synchrotron continuum,” *MNRAS*, 346, 885
- Smith, N. 2013, “The Crab nebula and the class of Type II_n-P supernovae caused by sub-energetic electron-capture explosions,” *MNRAS*, 434, 102
- Smith, N., Li, W., Filippenko, A. V., & Chornock, R. 2011, “Observed fractions of core-collapse supernova types and initial masses of their single and binary progenitor stars,” *MNRAS*, 412, 1522
- Soderberg, A. M., Chakraborti, S., Pignata, G., et al. 2010, “A relativistic type Ibc supernova without a detected γ -ray burst,” *Nature*, 463, 513
- Thorstensen, J. R., Fesen, R. A., & van den Bergh, S. 2001, “The Expansion Center and Dynamical Age of the Galactic Supernova Remnant Cassiopeia A,” *AJ*, 122, 297

- Vogt, F., & Dopita, M. A. 2011, “The 3D structure of N132D in the LMC: a late-stage young supernova remnant,” *Astrophysics and Space Science*, 331, 521
- Watson, D., Christensen, L., Knudsen, K. K., et al. 2015, “A dusty, normal galaxy in the epoch of reionization,” *Nature*, 519, 327
- Wongwathanarat, A., Müller, E., & Janka, H.-T. 2015, “Three-dimensional simulations of core-collapse supernovae: from shock revival to shock breakout,” *A&A*, 577, A48
- Woosley, S. E. 2010, “Bright Supernovae from Magnetar Birth,” *ApJL*, 719, L204
- Yang, H., & Chevalier, R. A. 2015, “Evolution of the Crab Nebula in a Low Energy Supernova,” *ApJ*, 806, 153
- Young, P. A., Fryer, C. L., Hungerford, A., et al. 2006, “Constraints on the Progenitor of Cassiopeia A,” *ApJ*, 640, 891